PERGAMON

Materials Science in Semiconductor Processing 1 (1998) 75–82

MATERIALS SCIENCE IN SEMICONDUCTOR PROCESSING

Incidence angle distributions of ions bombarding grounded surfaces in high density plasma reactors

E.S. Aydil[a,*], B.O.M. Quiniou[b], J.T.C. Lee[c], J.A. Gregus[c], R.A. Gottscho[d]

[a]*Chemical Engineering Department, University of California Santa Barbara, Santa Barbara, CA 93106, U.S.A.*
[b]*Lawrence Livermore National Laboratory, 7000 East Avenue, P.O. Box 808, Livermore, CA 94550, U.S.A.*
[c]*Bell Laboratories, Lucent Technologies, 600 Mountain Avenue, Murray Hill,, NJ, U.S.A.*
[d]*Lam Research Corporation, 4650 Cushing Parkway, Fremont, CA 94538-6470, U.S.A.*

Abstract

Ion incidence angle distribution on surfaces in plasma etching reactors determines the shape evolution of via holes and trenches through its effects on the spatial variation of ion fluxes along the walls of these microscopic features. We describe a novel retarding-field energy analyzer design that is capable of measuring the energy and the incidence angle distributions of ions bombarding grounded surfaces in plasma reactors with sub-0.5° resolution. Using this analyzer we measured the energy and angle distributions of Ar ions incident onto a Si surface in a low-pressure helicon wave excited Ar plasma. Ion angle distributions are approximately Gaussian. In absence of collisions in the sheath, the width of the ion angle distribution function is determined by the ratio of the directed energy gained in the sheath to the random ion energy in the plasma. Variation of the ion angle distribution width as a function of plasma power and pressure is determined by the dependence of the sheath potential and the ion temperature on these externally controlled parameters. In low pressure Ar plasmas, the ion angle distribution broadens with increasing power and shows a maximum as a function of pressure in the range 0.5–4 mTorr. © 1998 Elsevier Science Ltd. All rights reserved.

1. Introduction

Plasma etching has become a ubiquitous process in microelectronics because of its ability to transfer patterns from a mask onto an underlying film with precision unequalled by other etching methods. This precise pattern transfer is due to energetic ions bombarding the film surface primarily in the direction normal to the substrate. Ion bombardment enhances the etch rate in the direction normal to the surface allowing one to anisotropically etch narrow holes and trenches on thin films. In addition, the important role of ions in high density plasma chemical vapor deposition (HP-CVD) has also been shown [1, 2]. In HP-CVD reactors, angle and energy distributions of ions determine the feature topography evolution during the filling of the gaps between the metal lines with SiO_2 or fluorinated SiO_2 [1].

Energy and angular distributions of ions striking a substrate surface are amongst the most important parameters in plasma etching. The energy distribution of the ions incident onto a surface determines the rate of surface reactions and, therefore, affects etch rate and selectivity with respect to a mask or an underlying film. In addition, the ion incident angle distribution determines the spatial variation of the ion flux along the walls of a feature that is being etched. If the ions have a narrow distribution of incidence angles around the normal to the substrate surface then most ions strike the bottom of the feature. In contrast, mask undercutting, bowing and loss of anisotropy may result if the distribution is widely dispersed about the normal. Thus, ion energy and angular distribution functions play a central role in the degree of anisotropy achieved in plasma etching [3]. Current integrated cir-

* Corresponding author.

1369-8001/98/$19.00 © 1998 Elsevier Science Ltd. All rights reserved.
PII: S1369-8001(98)00003-1

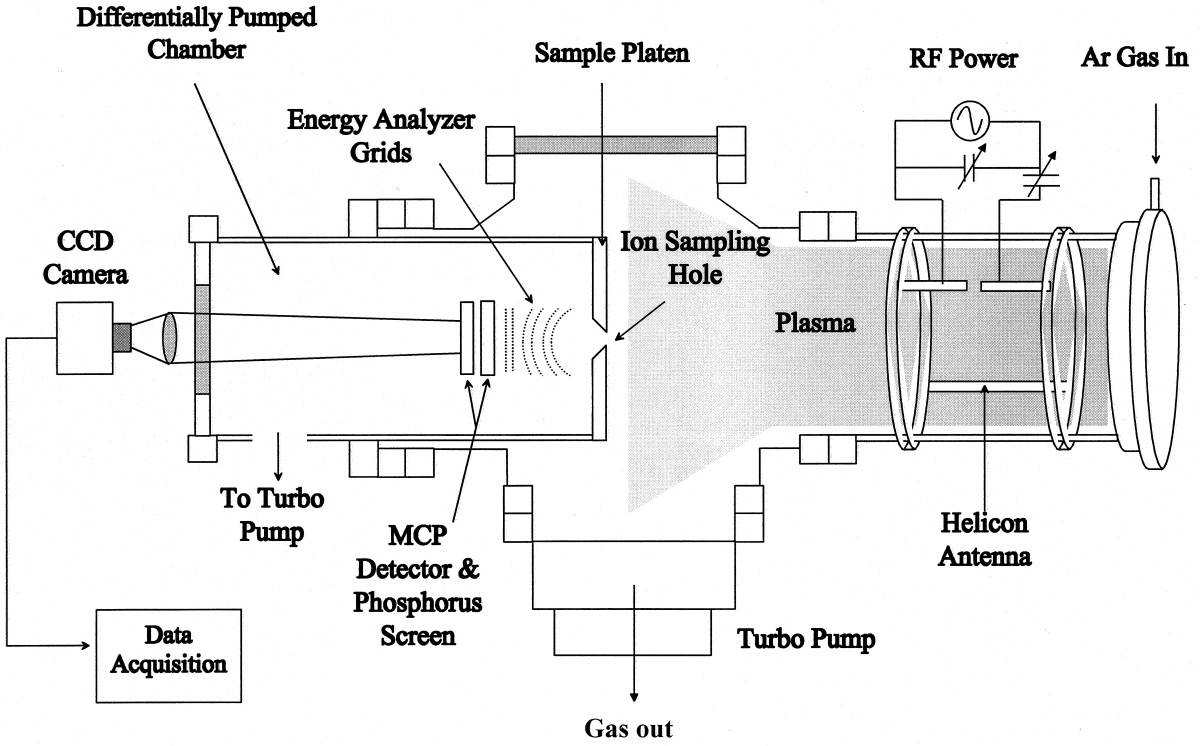

Fig. 1. Schematic of the helicon plasma source, the plasma reactor, and the differentially pumped chamber that houses the ion energy and angle distribution measurement apparatus.

cuit manufacturing technology requires narrow ion incidence angle distributions striking the substrate surface to etch high aspect ratio (depth to width) features with widths $<0.25\ \mu$m. Future integrated circuits are expected to have even smaller widths ($<0.18\ \mu$m).

2. Review of previous work

Starting with Coburn [4–7] in the 1970 s, numerous studies have focused on measurement of the ion energy distribution function (IEDF) in various plasma reactors and under different discharge operating conditions [8–11]. After the recognition of the importance of the ion energies, the experiments in the 1970 s and 1980 s concentrated on measuring the IEDFs without much attention to the angular distribution of the ions. In fact, the first experimental study of the angular distribution of ions striking a surface did not appear until 1990 [12]. Using a Faraday cup that consisted of isolated annular rings, Liu et al. [12] studied the angular distribution of ions incident onto the grounded electrode of a parallel plate plasma reactor in an Ar discharge. With their sectioned Faraday cup, Liu et al. achieved an angular resolution of 4.5°. More recently, Janes and Huth measured the energy-resolved angular distributions of O^+ and O_2^+ ions with 1° resolution using a mass spectrometer in conjunction with ion transfer optics which were placed immediately behind the powered electrode of a parallel plate reactive ion etching reactor [13–15]. These studies gave insight into the structure of the ion incidence angle distributions in parallel plate plasma reactors. However, despite the wide spread use of retarding field energy analyzers to study IEDFs, the more difficult IADF measurements are still scarce.

Since the current plasma etching technology requires etching of features with widths $<0.25\ \mu$m, a very narrow distribution of ion incident angles with full width at half maximum $<5°$ to 10° is desired [16]. Clearly, an IADF measurement method with improved resolution is needed. In this paper, we describe a retarding-field energy analyzer that is capable of measuring the ion angle distributions with better than 0.5° resolution. Using this analyzer, we studied the IEDFs and IADFs bombarding a grounded Si surface in a low-pressure high-density helicon plasma reactor in an Ar discharge.

3. Experimental apparatus and procedures

The experiments were conducted in the downstream region of a high density helicon wave excited plasma

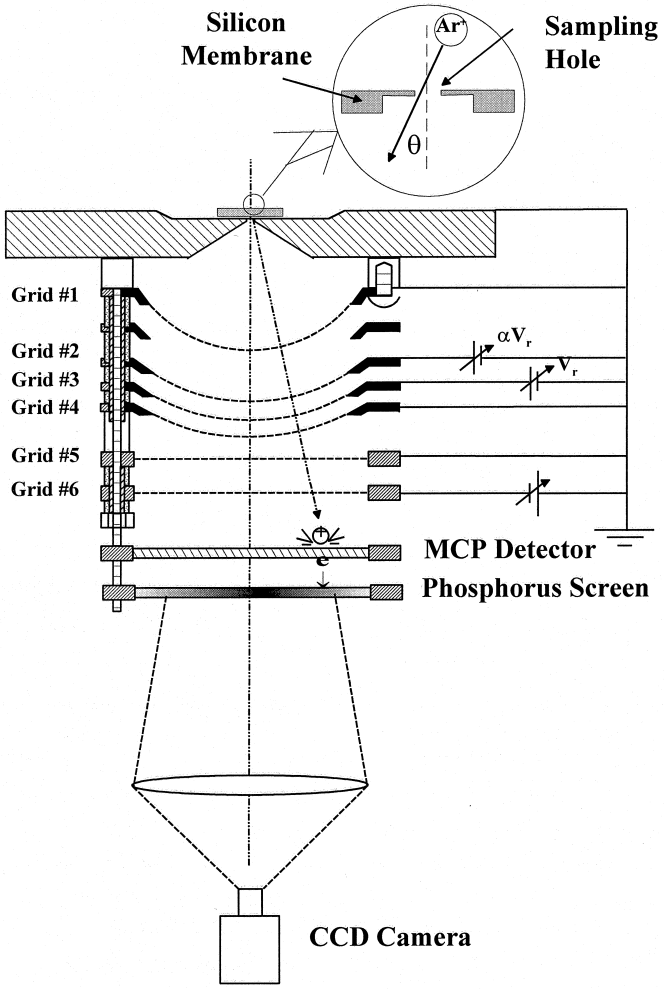

Fig. 2. Schematic of the retarding-field energy analyzer and the position sensitive detector for simultaneous measurement of the ion energy and angle distribution functions.

shown schematically in Fig. 1. The plasma reactor chamber was the same one that was previously used for studying ion and metastable atom transport in the source and reactor regions of electron cyclotron resonance and helicon-wave driven discharges [17–21]. The plasma chamber was pumped by a 1500 l sec^{-1} Turbo molecular pump and had a base pressure of 10^{-7} Torr. The pressure in the chamber was measured by capacitance manometers but not actively controlled. The Ar flow rate was regulated using a mass flow controller and fed into the reactor from the top of a quartz tube that, along with the helicon antenna, forms the plasma source. The plasma was maintained in the quartz tube by applying radio frequency (RF) power at 13.56 MHz to a helicon antenna through a matching network. The plasma expands from the quartz tube, the source region, into a stainless steel vacuum chamber referred to as the reactor region. The wafers would normally be placed on a substrate platen in the reactor region, facing the plasma expanding from the source.

For the ion energy and angle distribution measurements, a hollow differentially pumped chamber replaced the substrate platen of the reactor described above. The top surface of this chamber played the role of the substrate platen. Fig. 2 shows a detailed schematic of the differentially pumped chamber and the retarding-field energy and angle distribution analyzer housed in this chamber. The ions incident onto the substrate plane are sampled through a single circular via hole that connects the plasma chamber to the differentially pumped analysis chamber. The via holes used in this study were 50 μm in diameter and were produced on 35 μm thick, 5 mm × 5 mm square Si membranes on 20 mm × 20 mm Si dies. The Si dies

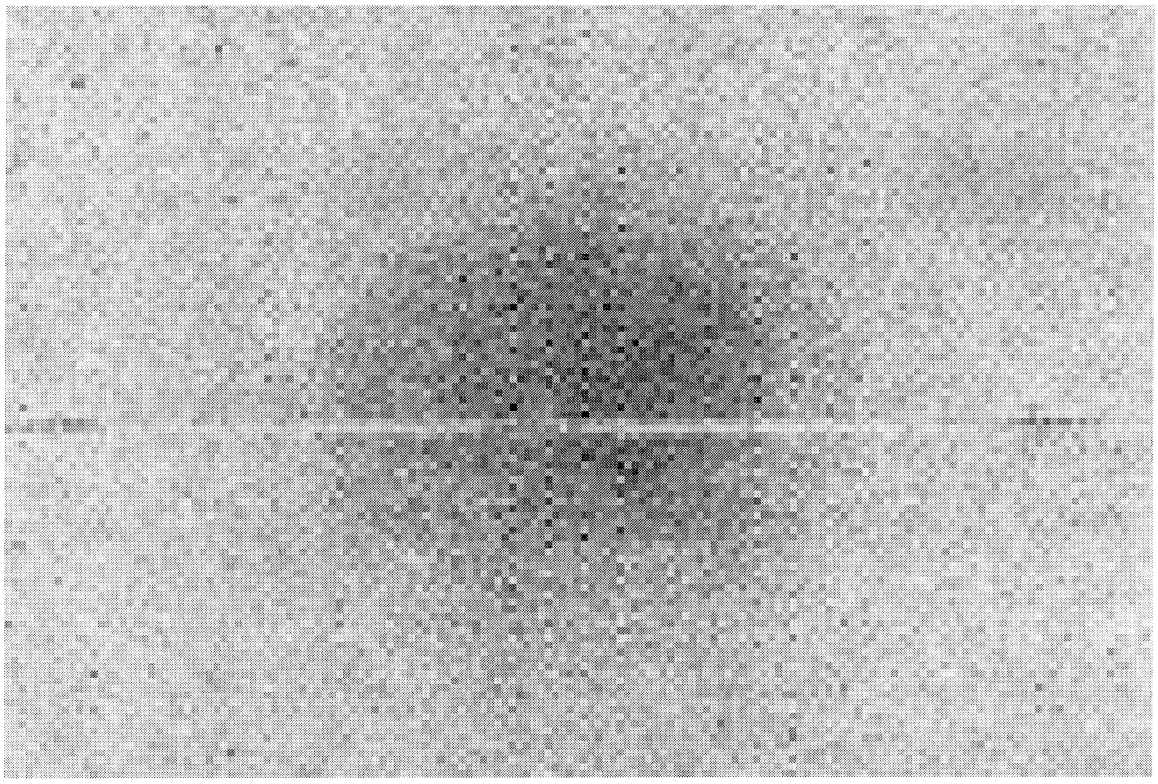

Fig. 3. A typical recorded and digitized image of the ions hitting the phosphorus plate. The plasma is maintained at 2 mTorr with 0.5 kW of RF power. The retarding potential, V_r is 12 V. The line drawn through the center is a typical section used to obtain the averaged distributions shown in Fig. 5. Many such lines were drawn through the center of the image at different polar angles to obtain the ion incidence angle distributions.

with the sampling hole were placed into a recessed groove on the center of the sample platen and mechanically clamped to ensure good thermal contact. Circulating cooling water through a channel recessed into the substrate platen cooled the membranes. The pressure in the differentially pumped chamber was maintained at 10^{-7} Torr to eliminate ion collision with gas molecules after they have passed through the sampling hole. In fact, both the plasma chamber (0.5–5 mTorr) and the analysis chamber pressure are low enough that the ion motion is essentially collisionless from the time they enter the platen sheath to the time they are detected.

Ion energies are analyzed using a retarding grid analyzer that consists of four hemispherical grids and two flat grids in the stacking configuration shown in Fig. 2. The top grid, labeled grid 1, is equipotential with the substrate platen and both of them are grounded to create a field free region immediately below the sampling hole. Grids 2 and 3 are biased at a positive potential and used to discriminate and repel the ions that have energies below the potential applied to grid 3, V_r. Two grids are used to provide a smooth repulsive barrier and to improve the energy resolution of the ionizer. Grid 2 is biased at a potential αV_r where $\alpha < 1$. Grids 4 and 5 are maintained at the same potential to provide a field free region between the flat grids and the hemispherical grids. Grid 6 is biased at a negative potential to repel the electrons sampled through the hole with the ions. After grid 6, the ions are accelerated towards a microchannel plate detector (MCP) placed 7 cm from the sampling hole. Since the distance between grids 5 and 6 and grid 5 and the MCP detector are very small compared to the distance between the sampling hole and the detector, the change in the trajectory of the ions between grids 5 and 6 is very small. Each ion striking the top of the MCP detector creates a localized electron avalanche that travels through the channels of the MCP. Thus the MCP amplifies the ion current while preserving the information about where the ion struck the MCP surface. The electrons emerging from the opposite end of the MCP detector are accelerated towards a phosphorus coated plate and excite phosphorescence at the same location that the original ion hit the MCP detector. A CCD camera placed outside the vacuum records the

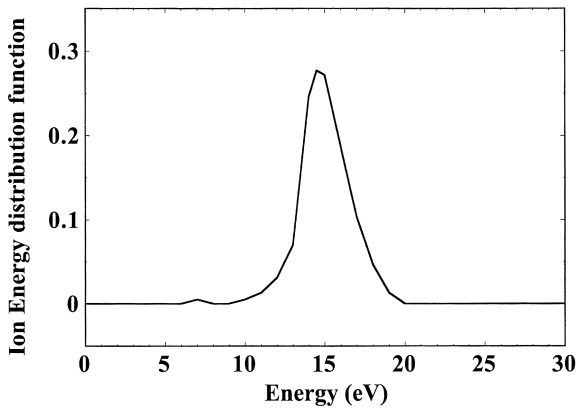

Fig. 4. Angle integrated ion energy distribution function recorded under the plasma conditions of Fig. 3.

phosphorescence image through a lens. This imaging method provides a projection of the locations of the ions striking the MCP detector. The ion incidence angle with respect to the normal to the platen surface is related to the ion impingement location on the MCP through simple geometry. Since the brightness at a particular location on the image is proportional to the time averaged flux of the ions striking the MCP, an image recorded with the ion retarding potential set at V_r is the energy averaged ion angle distribution functions from eV_r to infinity. The quantitative ion angle distribution functions are determined by grabbing, digitizing and analyzing the image. The locations with respect to the pinhole and size of the image are calibrated using an alignment cross, patterned onto the phosphorus screen.

A conservative estimate of the analyzer's angular resolution shows that it is $<0.5^\circ$. We estimate that the deviation introduced to the ion trajectory between grids 5 and the MCP detector is 0° when $\theta = 0^\circ$ and -0.3° when $\theta = 5^\circ$, increasing with increasing θ. Another source of loss of resolution is the smearing of the ion incidence location due to cross talk between the MCP channels, which were 0.25 μm in diameter. However, this effect is negligible compared to other sources of error. A typical spatial resolution of 0.1 mm on the MCP detector translates into an uncertainty $<0.1^\circ$ in the incidence angles of the detected ions. Finally, a resolution loss is incurred when the image created on the phosphorus screen is pixelized and digitized. Typical images consisted of 128×128 pixels that spanned an area that was *ca* 5 cm × 5 cm. Thus, a single pixel represents a signal averaged over a 0.3° angle. Based, on these calculations we estimate that this analyzer has a resolution better than 0.5°. Unfortunately, determining the true resolution requires an ion source that can produce ions with angular distribution widths $<0.5^\circ$ and such a source is not readily available.

4. Experimental results

Fig. 3 shows a typical image of the ions striking the MCP detector as projected onto the phosphorus screen and recorded by the CCD camera. The image was recorded while maintaining an Ar plasma at 2 mTorr with 0.5 kW of RF power. The retarding potential was set at 12 V to repel all ions that have energies <12 V. Under the conditions of the experiment in Fig. 3, almost all the ions have energies above 12 V. Thus the image represents the energy integrated angular distributions of ions passing through the hole. Except for small fluctuations in the brightness as a function of the position on the detector, the images appeared axisymmetric with respect to the polar angle, ϕ, of a coordinate system on the detector plane whose origin is the projection of the pinhole onto this plane. While there is no reason to expect the images to be axisymmetric we chose to focus on distributions with respect to the ion incidence angle, θ, by averaging intensities along many different lines drawn through the center of the bright spot, at different polar angles, ϕ, as shown in Fig. 3. In principle, imperfections in the via hole walls, as well as differential charging of the feature sidewalls can produce asymmetries in the ion angle distribution observed below the hole. Such effects should even be more pronounced if the via hole has a high aspect ratio. In fact, the high ion flux sensitivity and resolution of this technique allows one to study such subtle effects as distortion of ion angle and energy distribution functions by the feature. Herein, we limit our study to features with low aspect ratio (0.7). In the limit that the aspect ratio approaches zero and the hole diameter is on the order of or smaller than the Debye length, one obtains the angle and energy distributions incident onto the substrate surface. These conditions are satisfied in our studies where the Debye length 20–50 μm is on the same order as the sampling hole diameter (50 μm).

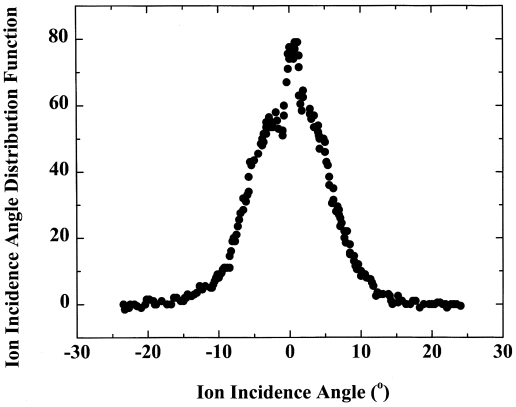

Fig. 5. Ion incidence angle distribution function determined from the image shown in Fig. 3.

Fig. 4 displays the energy distribution function of the ions imaged in Fig. 3. The maximum ion energy is 17 V indicating that this value is also the maximum plasma potential. Fig. 5 shows the ion incidence angle distribution function obtained from Fig. 3. The ion energy distribution has a Gaussian shape except for very small angles near normal incidence where a second, narrower distribution seems to be superimposed on the broader distribution. While this narrower component can be due to a cooler population of ions than the broad distribution, its width is approaching our spatial resolution and we cannot overlook the possibility that this feature may be an artifact of small variations in the radius of curvature of the spherical grids. Herein, we focus on the variation of the broader peak with the plasma conditions.

The ion angle distribution function is expected to be approximately Guassian, when the sheaths are collisionless and the energy gained in crossing the sheath is much larger than the random energy of the ions before they enter the sheath. Under these conditions, Gottscho [16] showed that the ion angle distribution function is given by

$$f(\theta) \approx C_N \exp(-\beta\theta^2) \tag{1}$$

where C_N is the normalization constant and β is the ratio of the directed energy gained in the sheath to the random ion energy in the plasma. The parameter β determines the width of the ion angle distribution function and is given by

$$\beta = \frac{eV_s}{kT_+} \tag{2}$$

where T_+ is the ion temperature that characterizes the random ion energy in the plasma. The full width at half maximum, $\Delta\theta_{FWHM}$, of the measured distribution functions are related to β by

$$\Delta\theta_{FWHM} = 2\sqrt{\frac{\ln 2}{\beta}} \tag{3}$$

From the width of the distribution function displayed in Fig. 4 (10.4°) we calculate β to be 84. Under these conditions the measured sheath potential is 17 V (see Fig. 4) which yields $kT_+ = 0.2$ eV. This value is typical of ion energies measured using Doppler shifted laser induced fluorescence of the N_2^+ and Ar^+ ions under similar conditions in high density plasmas [19, 20, 22, 23].

Fig. 6 shows the widths (full width at half maximum) of the ion angle distribution functions such as the one shown in Fig. 5, as a function of plasma power and pressure. As the pressure is increased from 0.5 mTorr, the widths of the IADF show a maximum *ca* 2 mTorr and decrease as a function of pressure. At a given pressure, increasing the plasma power increases the width of the IADF. The trends shown in Fig. 6 are counterintuitive at first glance because of the expectation that increasing pressure would broaden the IADF through collisions with the neutrals as the ions fall through the sheath. However, even at 4 mTorr, the mean free path of the ions is *ca* 0.8 cm, still much larger than the sheath thicknesses, which range from 0.01 to 0.05 cm depending on the plasma power. Sheath thicknesses were estimated from the measured plasma potentials (highest measured ion energy in an IEDF) using a simple model of the sheath [24]. Since the ions are accelerated through the sheath without collisions, the variation of the IADF widths must be understood in terms of the variation of the parameter β with power and pressure. Thus, the trends in the IADF width in Fig. 6 reflect the pressure and power dependence of the sheath potential, V_s and the ion temperature, T_+.

The sheath potential, V_s, in an Ar plasma is given by $V_s = 4.7\ kT_e/e$, where T_e is the electron temperature

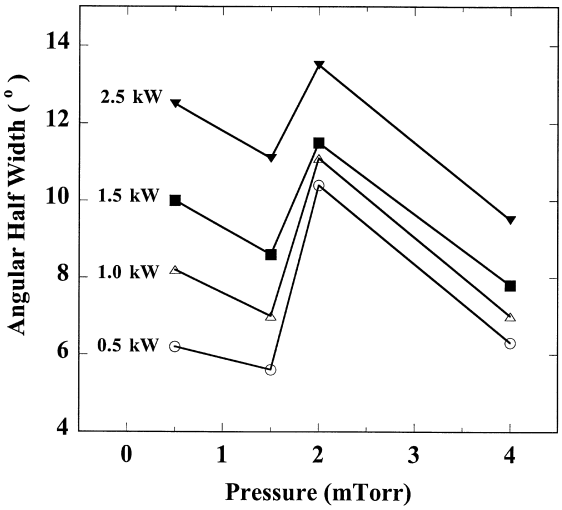

Fig. 6. Full width at half maximum of the ion energy distribution function as a function of pressure and power.

and k is the Boltzmann constant. A simple balance between the ion production by ionization and loss by recombination on the walls yields [25, 26]

$$\frac{k_i(T_e)}{\sqrt{kT_e/M_+}} = \frac{1}{N\Lambda} \tag{4}$$

where N is the neutral density, Λ is the reactor characteristic length and k_i is the ionization rate constant. If the dependence of the ionization rate constant on the electron temperature is known this equation can be solved to yield an estimate of the average electron temperature in the plasma. In an Ar plasma, the electron temperature and the plasma potential decrease with increasing neutral density. The dependence of the ion temperature on the neutral density and power is complex but, in general, the ion temperature increases with power and decreases with neutral density as charge exchange and other collisions with neutrals cool the ions. Since both the numerator and the denominator of the parameter β decreases with neutral density, the dependence of the IADF width is determined by the details of how V_p and T_+ vary with decreasing N. The situation is complicated by the fact that significant gas heating may also affect the neutral density at constant pressure [27], and pressure, measured at a single point downstream from the discharge, may not be representative of the gas density in the reactor. Furthermore, in high-density plasmas, the neutral density may be a function of position in the reactor [28, 29]. All these complications preclude simple explanation and prediction of the behavior of the IADF widths with changing power and pressure. Nevertheless, one can still understand some of the changes in Fig. 6 in terms of changes in β with variations in power and pressure. Simple but relatively accurate models of the plasma predict that the electron temperature and the plasma potential are independent of power. Thus, the increase in the width of the IADF with increasing power is attributed to increased ion heating and higher T_+. Hotter ion temperature at high RF power is either due to more intense fields in the plasma or due to decreased N and mean free path between collisions: at constant pressure, gas heating would result in a neutral density decrease. If one ignores gas heating and assumes that the neutral density is approximately proportional to the pressure, the general decreasing trend in the IADF with increasing pressure can be understood in terms of T_+ decreasing faster (α $1/N$) than V_p which decreases approximately logarithmically (α ln N). However, this mechanism alone does not explain the maximum in the IADF width at 2 mTorr. Sophisticated models that take into account the details of ion creation, heating and transport in high density plasma reactors are needed to fully understand the changes displayed in Fig. 6.

5. Summary, conclusions and future work

In summary, we have designed and built an apparatus that is capable of measuring the ion energy and incidence angle distributions bombarding surfaces in plasma reactors with unprecedented resolution. The apparatus was used to determine the ion angle distributions incident onto a grounded surface placed in the downstream of a helicon wave excited high density plasma source. The ion angle distributions were approximately Guassian and the width of the distribution function depends on power and pressure. In absence of collisions in the sheath, the ratio of the directed energy

gained in the sheath to the thermal energy of the ions in the plasma determines the IADF widths.

In practical etching and deposition processes, the substrate is biased with RF power. The method described herein can be extended to measurements of the IEDF and IADF incident onto rf-biased substrate electrodes. To accomplish this, the d.c. potentials applied to the various components of the analyzer must be with respect to the RF potential on the substrate electrode, using the electrode potential as a virtual ground. A method for accomplishing this and the electronics will be described in a future publication [30]. The data provided herein should be helpful in validating plasma simulation models that can predict ion angle distributions as a function of externally controlled plasma parameters such as power and pressure.

Acknowledgements

This work was performed as a part of a Cooperative Research and Development Agreement between Bell Laboratories and Lawrence Livermore Laboratories. The authors acknowledge fruitful discussions with Drs Dale Ibbotson of Lucent Technologies and Norman Bardsley of Lawrence Livermore Laboratories. E. A. also acknowledges funding from the National Science Foundation through a National Young Investigator Award (ECS9457758). We would like to thank Erik Edelberg and Sang Han for their help in the preparation of the manuscript.

References

[1] Shufflebotham MWP, Pirkle D, Denison D. Mater. Sci. Forum 1993;255:140–2.
[2] Han SM, Aydil ES. J. Vac. Sci. Technol. A 1996;14:2062.
[3] Gottscho RA, Jurgensen CW, Vitkavage DJ. J. Vac. Sci. Technol. B 1992;10:2133.
[4] Coburn JW. Rev. Sci. Instrum. 1970;41:1219.
[5] Coburn JW, Kay E. J. Appl. Phys 1972;43:4965.
[6] Kohler K, Coburn JW, Horne DE, Kay E, Keller JH. J. Appl. Phys 1985;57:5966.
[7] Coburn JW. Thin Solid Films 1989;171:65.
[8] Bohm C, Perrin J. Rev. Sci. Instrum. 1993;64:31.
[9] Ingram SG, Braithwaite NSJ. J. Phys. D: Appl. Phys. 1988;21:1496.
[10] Manenschijn A, Jansses GCAM, Van der Drift E, Radelaar S. J. Appl. Phys. 1991;69:1253.
[11] Thompson BE, Allen KD, Richards AD, Sawin HH. J. Appl. Phys. 1986;59:1890.
[12] Liu J, Huppert GL, Sawin HH. J. Appl. Phys. 1990;68:3916.
[13] Janes J, Huth C. J. Vac. Sci. Technol. A 1992;10:3522.
[14] Janes J, Huth C. J. Vac. Sci. Technol. A 1992;10:3086.
[15] Janes J, Huth C. Appl. Phys. Lett. 1992;61:261.
[16] Gottscho RA. J. Vac. Sci. Technol. 1993;11:1884.
[17] Giapis KP, Sadeghi N, Margot J, Gottscho RA, Lee TCJ. J. Appl. Phys. 1993;73:7188.
[18] Nakano T, Sadeghi N, Gottscho RA. Appl. Phys. Lett. 1991;58:458.
[19] Nakano T, Sadeghi N, Trevor DJ, Gottscho RA, Boswell RW. J. Appl. Phys. 1992;72:3384.
[20] Sadeghi N, Nakano T, Trevor DJ, Gottscho RA. J. Appl. Phys. 1991;70:2552.
[21] Trevor DJ, Sadeghi N, Nakano T, Derouard J, Gottscho RA, Foo PD, Cook JM. Appl. Phys. Lett. 1990;57:1188.
[22] Hartog EAD, Persing H, Woods RC. Appl. Phys. Lett. 1990;57:661.
[23] Wood RC, McClain RL, Mahoney LJ, Hartog EAD, Persing H, Hamers JS. SPIE 1991;1594:366.
[24] Economou DJ, Evans DR, Alkire RC. J. Electrochem. Soc. 1988;135:756.
[25] Lieberman, M.A., Lichtenberg, A.J.. Principles of Plasma Discharges and Materials Processing. New York: Wiley, 1994.
[26] Lieberman, M.A., Gottscho, R.A. In: M.H. Francombe, J.L. Vossen, editors. Physics of Thin Films. New York: Academic Press, 1994;vol. 18.
[27] Jarnyk MA, Gregus JA, Aydil ES, Gottscho RA. Appl. Phys. Lett. 1993;62:2039.
[28] Kilgore MD, Daugherty JE, Porteous RK, Graves DB. J. Vac. Sci. Technol. B 1994;12:486.
[29] Kilgore MD, Wu HM, Graves DB. J. Vac. Sci. Technol. B 1994;12:494.
[30] Edelberg, E.A., Perry, A., Benjamin, N., Aydil, E.S. unpublished.